PHYSICAL REVIEW D

PARTICLES AND FIELDS

THIRD SERIES, VOL. 2, NO. 3 1 AUGUST 1970

Asymmetric Electron Pair Production on Carbon*†

R. M. SIMONDS‡
High Energy Physics Laboratory, Stanford University, Stanford, California 94305

AND

B. RICHTER
Stanford Linear Accelerator Center, Stanford, California 94305

(Received 13 April 1970)

The cross section for the reaction $\gamma+C \rightarrow e^+ + e^- + C$ has been measured for a series of kinematic points giving nuclear momentum transfers in the region 0.2–0.7 F^{-2}, with incident photon energies in the region for photoproduction of the first two pion-nucleon resonances. Measurements were made, using asymmetric detection geometry, of electron and positron cross sections for each point. The charge-independent yields are shown to be in agreement with predictions of quantum electrodynamics for coherent and quasi-elastic production on carbon. The charge-asymmetric results are shown to be consistent with recent estimates of the interference between Bethe-Heitler and Compton pair production amplitudes with excitation of an intermediate π-N state in the Compton diagram.

I. INTRODUCTION

THE results of recent wide-angle electron pair production experiments,[1,2] performed to verify the predictions of quantum electrodynamics (QED), have been in general agreement with theoretical expectations[3] based on the point-interaction hypothesis of QED. These *symmetric* experiments detected both electrons and positrons at equal momenta ($p_\pm$) and at equal angles (θ) with respect to the incident photon beam. As a means of detecting possible deviations from the point-interaction theory, the symmetric geometry has the advantages that (1) the momentum transfer to the virtual electron is the same for both Bethe-Heitler graphs of Fig. 1(a), $q^2=(k-p_\pm)^2\approx -2k\cdot p_\pm$, (2) the momentum transfer at the nuclear vertex is relatively small, varying as $-p^2\theta^4$, such that the process is insensitive to the details of the nuclear interaction, and (3) the contribution from interference between Bethe-Heitler and Compton amplitudes, Figs. 1(b) and 1(c), is small.[4]

The *asymmetric* detection scheme treated by BDF[3] considered the detection of only one member of the electron pair; the unobserved lepton is produced preferentially in the forward direction. In this case, the momentum transfer to the virtual electron is physically interesting only for the Feynman diagram in which the detected lepton proceeds directly from the incoming photon vertex, in which case it varies as $q^2=-2k\cdot p$. If the detected lepton originates at the nuclear vertex, the virtual lepton is almost on the mass shell with $q^2\approx\mu^2$, and this diagram contributes an estimated 80% of the yield. Thus an experiment of relatively high accuracy is required to place a reliable limit on the off-the-mass-shell behavior of the electron propagator. A second

* Research sponsored by the U. S. Office of Naval Research Contract No. Nonr 225(67) and by the U. S. Atomic Energy Commission.

† This paper is based on a thesis submitted by one of the authors (R.M.S.) in partial fulfillment of the requirements for the degree of Doctor of Philosophy.

‡ Present address: Cambridge Electron Accelerator, Cambridge, Mass.

[1] J. G. Asbury, W. K. Bertram, V. Becker, P. Joos, M. Rhode, and J. S. Smith, Phys. Rev. **161**, 1344 (1967); E. Eisenhandler, J. Feigenbaum, N. Mistry, P. Mostek, D. Rust, A. Silverman, C. Sinclair, and R. Talman, Phys. Rev. Letters **18**, 425 (1967); and R. Weinstein, in Proceedings of the International Symposium on Electron and Proton Interactions, Stanford University, Stanford, Calif., 1967 (unpublished).

[2] K. J. Cohen, S. Homma, D. Luckey, and L. S. Osborne, Phys. Rev. **173**, 1339 (1968).

[3] S. D. Drell, Ann. Phys. (N. Y.) **4**, 75 (1958); J. D. Bjorken, S. D. Drell, and S. C. Frautschi, Phys. Rev. **112**, 1409 (1958). The latter will be denoted hereafter as BDF.

[4] Compton interference contributions vanish identically at exact symmetry as a consequence of Furry's theorem [see, for example, G. R. Henry, Phys. Rev. **166**, 1553 (1968)], and with finite experimental resolution, may be eliminated by not detecting charge, i.e., by detecting electrons and positrons for equal times in a given detector.

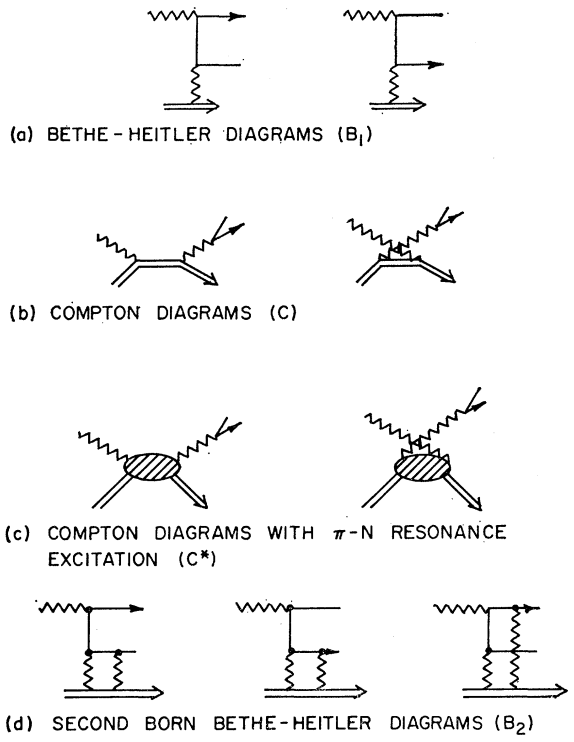

FIG. 1. Electron pair production diagrams.

feature of the asymmetric geometry is that the contributions from interference between Bethe-Heitler and Compton amplitudes do not vanish and can lead to a charge-asymmetric yield since the interference terms are odd under charge conjugation. Finally, for the asymmetric geometry, the momentum transfer to the target nucleus is relatively large, varying as $-p^2\theta^2$, which leads to the additional possibility of charge-asymmetric contributions from interference between first and second Born Bethe-Heitler amplitudes, Fig. 1(d).

The first asymmetric pair production experiment[5] observed only the 70-MeV positron produced at 90° in the laboratory by a bremsstrahlung beam with a peak energy of 137 MeV. The ratio of experimental to point-interaction theoretical cross section was found to be (0.96 ± 0.14), and no attempt was made to measure interference contributions. These were estimated by BDF, based on a Compton amplitude valid for incident photon energies well below threshold for excitation of the first pion-nucleon resonance, to be a factor of 10^{-4} lower than the direct yield from the square of the Bethe-Heitler amplitude.

More recently, asymmetric pair production[2,6] has been used as a means of obtaining the relative phase of ρ^0 amplitude at high energies by measuring the interference between Bethe-Heitler and Compton amplitudes for e^+, e^- masses in the region of the ρ resonance. In these experiments both members of the pair are detected at nearly symmetric angles, momenta, and transverse momenta, so that the momentum transfer at the nuclear vertex is close to that of symmetric detection.

However, in the intermediate energy range, where π-N resonances may dominate the Compton interference contributions, there have been no previous experimental or theoretical investigations. The purpose of the present work was to measure these terms below the threshold for ρ^0 production by studying the reaction

$$\gamma+\mathrm{C}\rightarrow e^+ + e^- + \mathrm{C}, \qquad (1)$$

using asymmetric detection geometry, one member of the pair being momentum analyzed by a magnetic spectrometer and detected by a counter telescope consisting of gas and plastic Čerenkov counters. Carbon electromagnetic form factors are well known from the extensive electron scattering work at Stanford[7]; the nucleus has spin 0, which simplifies calculations, and the low Z value minimizes second Born contributions to the experimental yield. The actual target material was polystyrene (CH), necessitating a small (5%) correction for pair production on protons in the plastic polymer chain.

Spurious events from protons, mesons, and muons were effectively eliminated by the Čerenkov counters, but appreciable background electrons from "double scattering" and from π^0 decays were measured and subtracted from the raw yields. Double-scattering events, comprising 30–40% of the total target-in yield, arose from pair production in the forward direction followed by a second elastic scattering into the detector acceptance. Events from neutral pion production followed by either internal Dalitz decay or external conversion of one of the decay photons from the more common decay mode constituted less than 10% of the total target-in yield. For both types of background, the fraction of events was determined experimentally. Loss of real positron events from annihilation in flight was a calculated correction to the experimental data.

Sections II and III describe the experimental apparatus and procedures. Section IV outlines the theoretical interpretations of the results in terms of recent calculations of Compton interference and first and second Born Bethe-Heitler interference contributions, and Sec. V presents a discussion of the results and conclusions.

II. EXPERIMENTAL APPARATUS

The energy-analyzed electron beam of the Stanford Mark III linear accelerator[8] was used with an energy spread of 1%. The beam-transport and energy-defining systems have been described elsewhere.[9] The primary energy calibration has been performed previously by

[5] B. Richter, Phys. Rev. Letters 1, 203 (1958).
[6] S. C. C. Ting, Lecture at the International School of Physics "Ettore Majorana," Erice (Trapani), Sicily, 1967 (unpublished).
[7] H. Crannell, Phys. Rev. 148, 1107 (1966); 136, B1580 (1964).
[8] R. B. Neal, Stanford University Microwave Laboratory Report No. 185, 1953 (unpublished).
[9] W. K. H. Panofsky and J. A. McIntyre, Rev. Sci. Instr. 25, 287 (1954).

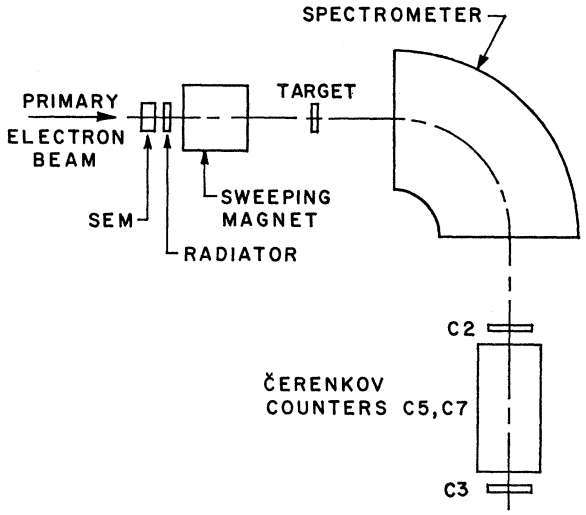

FIG. 2. Experimental apparatus.

floating-wire measurements and could be set to an estimated accuracy of 0.5%, using precision shunts monitoring analyzing-magnet currents.

The primary electron beam emerged from the accelerator drift tube and first passed through the secondary emission monitor (SEM) shown by Fig. 2. This device was the primary beam current monitor and consisted of five 0.25-mil aluminum foils, had an efficiency of approximately 8% with a small energy dependence, and was mounted on a wobbling base which prevented fatigue effects on the efficiency by moving the foils so that the roughly 0.25-in.-diam beam spot swept over an area of about 1 in.^{2}.

Following production of the bremsstrahlung beam in 0.0495 radiation lengths of copper foil, the residual electron beam was swept horizontally 20° to the right, passing through an air Čerenkov monitor into the beam catcher house. In order to minimize contamination of the photon spectrum, the sweeping-magnet gap was filled with a container of helium at atmospheric pressure. The air Čerenkov counter provided a monitor of beam current profile; it was periodically photographed for use in estimating dead-time corrections, and was supplied to the accelerator operator as an aid in obtaining a beam pulse as long as possible and reasonably free of violent fluctuations in electron density.

Positrons or electrons produced in a target of 0.995 g/cm^2 of polystyrene plastic were collimated by a 2.5×5 in.^{2} lead mask at the entrance to the spectrometer vacuum chamber, and the residual photon beam was absorbed by approximately 35 radiation lengths of lead stacked on one side of the spectrometer face. Lead and tungsten collimation was used along the air gap between the sweeping magnet and target to prevent possible scattering of charged secondaries into the spectrometer acceptance.

SEM efficiency was measured by comparison with a Faraday cup (not shown in Fig. 2) which could be rotated into the electron beam line at about the position of the spectrometer. When not in use, the Faraday cup was moved well out of the path of the photon or swept electron beams. Intercalibrations of the Faraday cup with other Stanford and SLAC beam monitors, described by several authors,[10] have indicated efficiency differences of less than 0.3%.

The spectrometer was an $n=0$, 90° bend magnet,[11] with a mean orbital radius of 44 in., mounted on a rotatable mount with provisions for remote angular adjustment and monitoring. The mean polar angle of the observed leptons was reproducible to within less than 0.05°, and the absolute calibration was verified with reference to the primary beam line fiducials to the same precision. The measured momentum dispersion of the spectrometer is $\Delta p/p=0.01$ per inch at the focal plane and the length of the defining counters gave a total momentum acceptance of about 8% (full width at half-maximum). Polar angle acceptance, determined by the counter width of 4 in. due to lack of magnet focusing in this direction, was about 0.02 rad.

Spectrometer fields were monitored by a lithium chloride nuclear magnetic resonance (NMR) probe with only moderate success. The proton resonance signal was usable at low momenta, but at momenta greater than 300 MeV/c, the low signal-to-noise ratio did not provide a reliable field monitor. In this case, the shunt voltage readout of the magnet current was used as a field monitor, and the shunt settings calibrated against the NMR signal with accelerator rf off. The NMR-shunt voltage correlations were verified to within 0.2% and it was found that the polarity of the magnet could be reversed, using shunt readout only, with the same degree of accuracy.

The detection system consisted of two Plexiglas Čerenkov counters, $C2$ and $C3$, and a double-chamber threshold gas Čerenkov counter, shown in Fig. 2. The gas Čerenkov counter is shown in detail in Fig. 3. Each plastic Čerenkov counter was made from 4×8×1-in.-thick ultraviolet transmitting Plexiglas with three Amperex XP1110 phototubes attached with epoxy resin to the 4×1-in. face of the plastic. The 4×8-in.^{2} surface of the counter was oriented normal to the incident beam direction to match the sensitive area of the gas counter. The anode pulse output of the three tubes was added directly in a linear fan-in circuit and the single output was amplified to obtain a usable signal level. The measured efficiency of the counters for detection of minimum-ionizing cosmic rays was 0.75, and, for the ranges of incident momenta, were sensitive to electrons and pions but rejected protons.

The gas Čerenkov counter (Fig. 3) was designed to provide a coincidence output from two optically inde-

[10] T. Janssens, Ph.D. thesis, Stanford University, 1965 (unpublished); D. Yount and J. Pine, Phys. Rev. **128**, 1842 (1962); D. Yount, Nucl. Instr. Methods **52**, 1 (1967).

[11] J. V. Allaby and D. M. Ritson, Rev. Sci. Instr. **36**, 607 (1965).

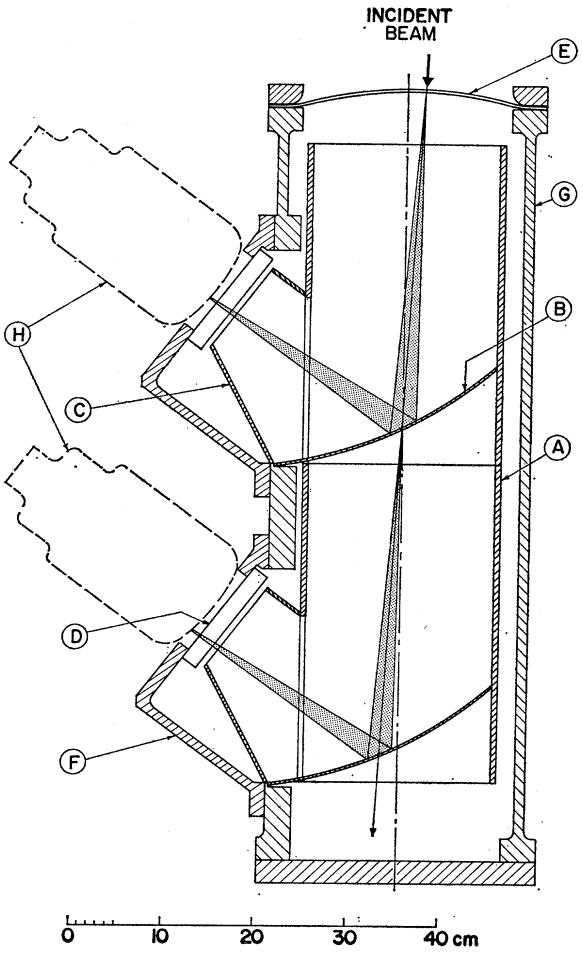

FIG. 3. Čerenkov-counter cross section in the median plane of the incident beam: (A) 10×20-cm light pipe, 7.5-mm-thick front-surface glass mirror, (B) 22-cm focal length aluminized Plexiglas spherical mirror, 2.0 mm thick, (C) aluminized Plexiglas light pipe, (D) Plexiglas II UVT window, 1.9 cm thick, (E) Mylar window, 15×0.19 mm thick, (F) light-port assembly, (G) 30.0-cm-diam aluminum tube, (H) Amperex 58AVP photomultiplier tube.

pendent chambers enclosed in a single gas envelope. The momentum-analyzed beam entered the counter through a window laminated from 15×0.0075-in.-thick Mylar film; the details of construction are described elsewhere.[12] The two chambers have identical optics and the spherical mirrors are fitted to the glass light pipe to eliminate light leaks between chambers. The gas dielectric is Freon 13 ($CClF_3$) at a pressure of 200 psig and a regulated temperature of 30°C. Under these conditions, the index of refraction is approximately 1.02, giving threshold for pions of 700 MeV/c and for muons of 525 MeV/c. By reducing gas pressure, the pion and muon thresholds may be increased with a loss in Čerenkov light yield from electron events. The optimum operating conditions were obtained by jointly varying pressure and phototube voltages to obtain a plateau in the electron detection efficiencies for the two chambers. Repeated measurements of individual chamber efficiencies for electron detection gave momentum-independent values of (0.94±0.03) and (0.92±0.03) for the first and second chambers, respectively, and the measured average pion/muon detection efficiency for both chambers was $(2\pm4)\times10^{-4}$.

As stated above, the SEM was used as the primary monitor of incident electron current. The output of the SEM was integrated by a conventional feedback-type integrator. The integrator capacitors have been calibrated previously against 0.1% precision standards, and the capacitors used for the present experiment were rechecked and the values verified to within 0.2%.

III. EXPERIMENTAL PROCEDURES

A. Photoproduction Experiment

Measurements were made of electron and positron events at seven kinematic points defined by spectrometer angle and momentum and peak bremsstrahlung energy, which gave nuclear momentum transfers in the range 0.2–0.7 F^{-2}. An event was defined by the coincidence $C3C5C7$; including $C2$ in the logic requirement did not increase the detection efficiency of the telescope. Hence, it was included only during efficiency and rejection ratio measurements. For a fixed peak photon energy and kinematic setting of the spectrometer, three to five yield measurements were made at each polarity, and target-out yields were measured after each target-in run. Following this, a series of copper foils, varying from 0.01 to 0.04 radiation lengths in thickness, were inserted in the photon beam ahead of the target in order to measure the linear increase in double-scattering events. Similarly, a series of aluminum foils was placed at the entrance of the spectrometer vacuum chamber to measure the contributions from multiple scattering and π^0 decay electrons or positrons.

SEM efficiency was calibrated against the Faraday cup at approximately 6-h intervals, or more frequently if primary electron energy had been altered. At least two measurements were made for each value of peak photon energy.

At the beginning and end of runs at one kinematic point, the sweeping magnet was turned off, and the primary electron beam allowed to strike the target with the spectrometer angle increased to a point at which pion electroproduction was kinematically forbidden. Under these conditions, momentum-analyzed electrons from inelastic scattering events in the target were used to measure gas Čerenkov counter efficiencies.

The efficiency of the gas counter for pions and muons was measured using the standard photoproduction experimental configuration and included the signal from the plastic counter $C2$ in the coincidence logic requirement. Using the electron detection efficiencies obtained from the procedure described above, values of efficiency

[12] R. Simonds and B. Richter, Rev. Sci. Instr. 34, 929 (1963).

for pion and muon detection were obtained which ranged from $(5\pm4)\times10^{-4}$ to $(0\pm5)\times10^{-4}$.

B. Data Reduction

The raw data consisting of *C3C5C7* coincidence events were normalized to the integrated primary beam current, corrected for accidental coincidence rates of about 1% measured by delayed logic channels, and for dead-time losses (<4%) induced by the electronic logic. Target-out background was subtracted, and the result expressed as events per volt, or equivalently, as events/1.003 μC of primary beam current. The three to five measurements at each polarity and each kinematic point were then averaged by maximum-likelihood methods to obtain the values of "observed yield" listed in Table I.

Subtraction of double-scattering and π^0 decay events was done in the following manner: In the absence of additional radiator foils in the photon beam, the observed lepton yield, after the corrections described above, may be expressed in the form

$$Y_0=\sigma_p t+\sigma_p'\sigma_s(\tfrac{1}{2}t+t_u)t+\sigma_0 t_d.$$

In this expression, σ_p is the electron pair production probability for asymmetric production at angle θ, σ_p' is the electron pair production probability at forward angles, σ_s is the elastic scattering probability at angle θ, σ_0 is the neutral pion production probability, t_u is the material ahead of the target, t_d is the material between the point of neutral pion production and the spectrometer vacuum chamber entrance, plus 1/80 for Dalitz decay probability, and t is the target thickness. All production probabilities are in units of (radiation length)$^{-1}$.

A simple calculation shows that the fraction of double-scattering events is given by the quantity

$$\frac{Y-Y_0}{Y}\frac{\frac{1}{2}t+t_u}{\tau},$$

where Y is the observed event rate with τ radiation lengths of foil added in front of the target. Similarly, the fraction of π^0 decay events is given by

$$\frac{Y-Y_0}{Y_0}\frac{t_d}{\tau},$$

where Y is the observed event rate with τ radiation lengths of foil added between the target and the spectrometer entrance. For most of the kinematic points investigated, the observed lepton energy was within 100 MeV or less of the peak energy of the bremsstrahlung spectrum which suppressed neutral pion production as compared with multiple scattering when radiators were added between the target and the spectrometer vacuum entrance window. In these cases, it was assumed that the relatively small negative slope of yield with radiator thickness was due entirely to multiple-scattering losses; the Dalitz decay probability was dropped from the sum of equivalent radiator thicknesses and the radiator subtractions carried out as usual with the appropriate change of sign. The resulting fractional values of π^0 or multiple-scattering loss for the two spectrometer polarities have been averaged, since there is no physical reason to suppose a charge asymmetry, and the data are statistically consistent with a single value. The double-scattering fractions, however, have not been averaged between polarities to allow for the possibility that an electron excess may be due to Compton electrons. The experimentally determined fractions for these background processes are listed in Table I.

TABLE I. Experimental results and corrections.

E_0 (MeV)	$p_\pm$ (MeV/c)	θ (deg)	Polarity	Expt yield[a]	Fractional correction factors Decay[b]	D.S.[c]	Annihilation[d]	Corr. net yield[e]
390.0	170.0	30.00	+	16.29±0.31	−0.063±0.052	−0.410±0.024	+0.018	8.74±0.95
			−	16.43±0.28		−0.456±0.025		7.90±0.96
	340.0	18.10	+	4.86±0.10	+0.077±0.034	−0.416±0.025	+0.0095	3.24±0.22
			−	6.94±0.14		−0.368±0.039		4.92±0.37
550.0	450.0	14.85	+	9.23±0.20	+0.125±0.032	−0.441±0.032	+0.0075	6.36±0.44
			−	10.66±0.29		−0.448±0.045		7.21±0.57
		20.40	+	1.74±0.04	+0.058±0.044	−0.415±0.050	+0.0075	1.13±0.12
			−	2.00±0.05		−0.377±0.046		1.36±0.13
715.0	625.0	10.15	+	15.94±0.36		−0.512±0.057	+0.006	7.82±0.92
			−	20.16±0.46		−0.326±0.108		13.59±2.20
		13.00	+	4.63±0.12	+0.053±0.040	−0.428±0.042	+0.006	2.91±0.28
			−	5.33±0.13		−0.466±0.037		3.16±0.30
		14.95	+	2.19±0.06	+0.058±0.046	−0.438±0.053	+0.006	1.36±0.16
			−	2.69±0.07		−0.334±0.048		1.94±0.19

[a] Observed events/volt corrected for accidentals, dead-time losses, and target-out background.
[b] Radiator subtraction for fractional yield due to π^0 decay leptons or multiple-scattering losses.
[c] Radiator subtraction for fractional yield from double-scattering events.
[d] Calculated fraction of positron annihilation in flight.
[e] Corr. net yield equals Expt yield corrected for the total fractional losses of items (b)–(d).
[f] Data not recorded. Calculation assumes zero contribution.

Corrections for positron annihilation in flight in the target or in material ahead of the spectrometer entrance are implicit in the radiator subtraction procedure; however, annihilation in the counter telescope has been computed from the Heitler total cross section[13] and the estimated thickness presented by the Čerenkov counters. The correction to the positron yields as given by Table I amounts to less than +2% for all kinematic points.

C. Normalization

The combined acceptance and detection efficiency of the counter telescope was determined by a measurement of the yield of electrons scattered inelastically from the same target as used for pair production. With a primary electron beam energy of 390 MeV, the spectrometer was adjusted to observe 170-MeV/c electrons scattered at 30° from the standard polystyrene target. Events originated from inelastic scattering and from double scattering, and, as in photoproduction runs, a sequence of copper radiators was inserted in the primary beam upstream of the target to measure the double-scattering component.

The yield remaining after subtraction of double-scattering events was due to wide-angle bremsstrahlung (WAB) events in which a real photon is emitted either before or after an elastic scattering event. For the present experimental conditions, a photon of about 220 MeV is radiated and the largest part of the yield of WAB events (97%) comes from radiation by the incoming electron followed by scattering at 170 MeV. The Berg-Lindner[14] cross section for this process, differential in the variables of the three final-state particles, has been integrated numerically by Allton[15] over the unobserved particle parameters; it has also been integrated by Hand[16] in the "peaking approximation." In the latter, it was assumed that the principal contribution to the yield arises from events in which photon emission is approximately collinear with the incident or final electron. With this simplification, the WAB cross section factors into products of the Rosenbluth elastic scattering cross section and kinematic factors. If E_1 (E_2) is the incident (final) electron energy, then

$$\frac{d\sigma}{d\Omega dE_2}=\eta_1^2\frac{\chi_1}{k_1}\frac{d\sigma}{d\Omega}(\theta,E_1')+\frac{\chi_2}{k_2}\frac{d\sigma}{d\Omega}(\theta,E_1), \tag{2}$$

in which

$$\eta_1=E_1'/E_2=[1-E_2(1-\cos\theta)/M]^{-1},$$

$$\eta_2=E_1/E_2'=1+E_1(1-\cos\theta)/M,$$

$$\chi_i=\left(\frac{\alpha}{\pi}\right)\left(\frac{\eta_i}{\eta}\right)\left[\ln\left(\frac{|q^2|}{\mu^2}\right)-1+\frac{k_i^2}{E_iE_i'}\ln\frac{2E_i}{\mu}\right],$$

$$i=1,2,\quad \eta=E_1/E_2,$$

$$k_1=E_1-E_1',\quad k_2=E_2'-E_2.$$

For c.m. energies below the first resonance, the peaking approximation has been found by Allton[15] to differ by less than 2% from a numerical integration of the exact Berg-Lindner formula over the phase space of the unobserved photon and lepton.

The WAB cross section has been calculated from Eq. (2) for interactions with C^{12} (95%) and with protons, both quasi-elastically on protons in carbon and on free protons in the target (5%). The percentages indicate the relative contributions. Radiative corrections, following Berg and Lindner, have been calculated from the expression given by BDF for the closely analogous process of electron pair production. Including these corrections of +5.6% the acceptance of the spectrometer was estimated as

$$\Delta\Omega\Delta p/p=1.71\times10^{-4}(1\pm0.04),$$

with errors due to statistics alone.

Since lepton momenta of the various experimental points extended from 170 to 625 MeV/c, corrections to the acceptance for multiple scattering in the counter telescope were calculated from the known thickness of Plexiglas and Freon 13 in the counter telescope. The analysis assumed that one-half of the gas counter material plus the thickness of counter $C2$ was concentrated at the location of $C2$, and a multiple-scattering distribution for this geometry was constructed from the work of Nigam.[17] A Monte Carlo computer simulation was used to calculate the average efficiency of the telescope for each value of spectrometer momentum. The calculated efficiencies are shown in Table II, along with the effective spectrometer acceptance obtained by normalizing the multiple-scattering efficiency to unity at the 170 MeV/c momentum point. Thus the multiple-scattering correction had the effect of increasing the relative acceptance of the telescope by as much as 28% at higher momenta.

The second-Born-approximation single-scattering cross section used by Nigam allows the computation of

TABLE II. Effective spectrometer acceptance.

Momentum (MeV/c)	Multiple-scattering efficiency	Effective acceptance $(\Delta\Omega\Delta p)_{\text{eff}}$
170	0.61	0.0290(1±0.04)
340	0.74	0.0708
450	0.77	0.0976
625	0.78	0.1376

[13] W. Heitler, *The Quantum Theory of Radiation*, 3rd ed. (Oxford U. P., London, 1964).
[14] R. A. Berg and C. N. Lindner, Phys. Rev. **112**, 2072 (1958).
[15] E. A. Allton, Phys. Rev. **135**, B570 (1964).
[16] L. N. Hand, Phys. Rev. **129**, 1834 (1963).
[17] B. P. Nigam, Phys. Rev. **131**, 238 (1963).

multiple-scattering distributions which differ depending on lepton charge. The difference was apparent in the derived distributions to the extent of one part in 10^4 but produced negligible difference between multiple-scattering corrections for electron and positron detection.

D. Experimental Results and Estimated Errors

A listing of the experimental results for the seven kinematic points is shown in Table I, in which the observed event rate has been corrected for dead-time losses, accidental coincidences, and target-out background, and normalized to the integrated primary beam current. The table also lists the fractional correction factors obtained experimentally for double-scattering events, for π^0 events or multiple-scattering losses and the calculated estimate of positron annihilation in flight. In the final column are listed the net experimental yield after the indicated corrections have been made. The errors include the statistical errors of the experimental data as well as the propagated statistical errors of the radiator subtractions.

Systematic errors and uncertainties, given in Table III, depend in part on the experimental result. The absolute pair production yields are subject to the usual uncertainties in primary beam, target, spectrometer, and detector parameters, but the experimental values of electron-positron asymmetry are uncertain only by the degree of accuracy with which the spectrometer polarity could be reversed. The remaining errors do not affect the asymmetry measurements.

The uncertainty in the normalization experiment consists of 4% from statistical errors in the measurement of the WAB cross section, and 2% uncertainty due to the use of the peaking approximation to the theoretical Berg-Lindner cross section. Uncertainties in the carbon form factors have been neglected since they will be canceled by similar errors in the calculation of the theoretical pair production rates. The effects of the calculated multiple-scattering corrections on the normalization are more difficult to analyze owing to the number and extended distribution of the counter elements. However, an extremely conservative estimate of a 20% uncertainty in the calculated multiple-scattering losses gives only a 5% uncertainty in the normalization, since the multiple-scattering efficiencies were normalized to unity at the 170-MeV/c normalization point.

In the pair production experiment, uncertainties in target density and thickness have been omitted since the same target was used for both pair production and normalization. Furthermore, since the Bethe-Heitler cross section, including carbon form factors, varies approximately as $p^{-4.5}\theta^{-6}$ the uncertainty induced by spectrometer angular and momentum tolerances are 3% and 2.2%, respectively, considering the $\frac{1}{2}$% uncertainty in absolute momentum calibration and 0.05° angular tolerance in spectrometer alignment.

TABLE III. Estimated systematic uncertainties.

Normalization	6.7%
Spectrometer angle	<3.0
Spectrometer momentum	2.2
Bremsstrahlung spectrum	3.0
Radiator subtractions	2.0
Beam current monitors and integrators	0.5
Dead-time corrections	0.4

The error in the bremsstrahlung spectrum comes from uncertainty in the copper radiator foil (1.5%), a correction for contributions from the SEM foils (2.5%), and a small uncertainty due to drift in the end-point energy of the photon spectrum (0.5%). Similarly, the error in radiator subtractions is due to uncertainties in the estimates of the thickness of extraneous material in the beam line and of the thickness of added radiators used to determine the fractional contributions from double-scattering and π^0-decay contributions.

Errors due to beam current monitors and integrators have been assigned the value of 0.5%, the observed fluctuation in measured values of the SEM efficiency. Linearity and stability of the integrators was about 0.1% and the observed fluctuations may be attributed to slight mis-steering of the primary beam during calibrations or to other minor experimental errors.

The major uncertainty in estimates of dead-time corrections came from the assumption that the primary-beam pulse length was stable. Long-term fluctuations of pulse length varied between 0.4 and 1.2 μsec and dead-time corrections for variations of this magnitude were based on the photographic records of beam pulse shape. Short-term fluctuations of ± 10% were common under the most ideal accelerator operating conditions, however, causing an estimated 0.4% uncertainty in the final results.

The quadratic combination of the various errors gives a total systematic uncertainty of less than 7.3% in the case of the pair production yields and the value of 3% from the reversibility of the spectrometer polarity applicable to the electron-positron asymmetry measurements.

IV. THEORETICAL ESTIMATES OF PAIR PRODUCTION

A. General Information

In this section, it is convenient to denote the amplitudes associated with the graphs of Fig. 1 by the following: B_1 is the first Born Bethe-Heitler amplitude, C is the Compton amplitude for an intermediate Dirac proton, C^* is the Compton amplitude with excitation of a resonant pion-nucleon intermediate state of a target nucleon, and B_2 is the second Born Bethe-Heitler amplitude. Then, as examples, the contribution to the cross section from the square of the first Born Bethe-Heitler amplitude is labeled as $B_1 \times B_1$, and the interference term between first and second Born Bethe-Heitler amplitudes as $B_1 \times B_2$. The notation is merely a

means of labeling the process or the resulting contribution to the cross section.

B. Contributions from B_1 and C Amplitudes

The BDF calculation of pair production represented an improvement on the original Bethe-Heitler[18] work by the inclusion not only of the Compton diagrams but also the effect of dynamical corrections from the proton current, the inclusion of general nuclear form factors, an estimate of radiative corrections, and estimates of the $B_1\times C$ and $C\times C$ contributions. The $B_1\times B_1$ contribution was carried out in sufficient generality to allow the use of arbitrary nuclear form factors, but in the construction of the Compton amplitude, the target was considered merely as a point Dirac particle with an anomalous magnetic moment. With this model, the $B_1\times C$ and $C\times C$ terms are expected to be valid only for incident photon energies well below the first π-N resonance.

The $B_1\times B_1$ cross-section differential in electron and positron variables was integrated by BDF over the variables of the unobserved lepton to obtain the cross section for the asymmetric experiment. The integration required an expansion of the nuclear form factors to second order in q^2/M^2. However, this expansion was not sufficient in the present calculations to represent the carbon form factors, since momentum transfers extended beyond the first diffraction minimum of the C^{12} form factors even for the lowest value of q^2 investigated. Hence, the BDF coincidence cross section has been used as a basis for estimating yields and was integrated numerically over unobserved lepton parameters.

The pair production differential cross section is[3]

$$\frac{d\sigma}{d\Omega_1 d\Omega_2 dp_1 dp_2}=\frac{\alpha^3 M}{4\pi^2}\frac{p_1^2}{E_1}\frac{p_2^2}{E_2}\frac{G(k)}{Q\cdot(p_1+p_2)-p_1\cdot p_2}\times(\lambda_{11}+\lambda_{12}+\lambda_{22}), \quad (3)$$

in which $G(k)$ is the laboratory photon spectrum and λ_{11}, λ_{12}, and λ_{22} are the contributions from $B_1\times B_1$, $B_1\times C$, and $C\times C$, respectively. The photon energy is given by

$$k=\frac{Q\cdot(p_1+p_2)-p_1\cdot p_2}{M-k\cdot(p_1+p_2)/|k|}$$

and

$$\lambda_{11}=\frac{1}{2q^4}f_1(q^2)\left[\left(\frac{\mu}{k\cdot p_1}\right)^2 q^2-2\left(\frac{k\cdot p_1}{k\cdot p_2}+\frac{k\cdot p_2}{k\cdot p_1}+\frac{q^2 p_1\cdot p_2}{k\cdot p_1 k\cdot p_2}\right)\right]+\frac{1}{2q^4}f_2(q^2)\left[2\left(\frac{\mu p_1\cdot P}{k\cdot p_2}\right)^2-q^2\frac{(p_1\cdot P)^2+(p_2\cdot P)^2}{k\cdot p_1 k\cdot p_2}\right]. \quad (4)$$

The remaining terms are defined by Table IV. The subscript 1 (2) denotes positron (electron) variables, and, with the exception of terms of order μ^2 which arise from simplifications made by BDF and not from inherent asymmetry of the $B_1\times B_1$ terms, the expression is symmetric under charge conjugation: $1\leftrightarrow 2$. Similarly, the $C\times C$ terms are even under charge conjugation and the $B_1\times C$ terms are odd; for the conditions of the present experiment, these contributions are factors of 10^{-5} and 10^{-3} lower than the $B_1\times B_1$ yield and are omitted from further consideration.

The form factors in Eq. (4) are given by BDF as

$$\frac{1}{Z^2}f_1(q^2)=\frac{q^2}{M^2}(F_1+\kappa F_2)^2+\frac{P^2}{2M^2}\left(F_1^2-\frac{\kappa^2 q^2}{4M^2}F_2^2\right),$$
$$\frac{1}{Z^2}f_2(q^2)=\frac{1}{M^2}\left(F_1^2-\frac{\kappa^2 q^2}{4M^2}F_2^2\right), \quad (5)$$

in which $F_1\equiv F_1(q^2)$ and $F_2\equiv F_2(q^2)$ are the Dirac and Pauli form factors. The form factors F_1 and F_2 are related to other form factors commonly used in describing electron-proton elastic scattering by the following:

$$F_{ch}=G_E=F_1-r\kappa F_2,$$
$$F_{mag}=G_M/(1+\kappa)=(F_1+\kappa F_2)/(1+\kappa),$$
$$r=|q^2|/(4M^2).$$

Using these relations, the approximation that $P^2\approx 4M^2$, and the fact that $G_M{}^2=0$ for carbon, Eqs. (5) become

$$\frac{1}{Z^2}f_1(q^2)=\frac{2G_E{}^2}{1+r},\quad \frac{1}{Z^2}f_2(q^2)=\frac{(G_E/M)^2}{1+r}. \quad (6)$$

Form factors for proton targets are obtained by defining $G\equiv G_{Ep}=G_{Mp}(1+\kappa)$, from which the following

TABLE IV. Symbols. (A metric is used such that $p_1\cdot p_2=E_1E_2-\mathbf{p}_1\cdot\mathbf{p}_2$.)

α	$=1/137$
M	=carbon mass
m	=proton mass
μ	=electron mass
κ	=proton anomalous magnetic moment
E_1, p_1	=energy, four-momentum of outgoing positron
E_2, p_2	=energy, four-momentum of outgoing electron
Q	=four-momentum of initial target nucleus
Q'	=four-momentum of final target nucleus
P	$=Q+Q'$
k	=four-momentum of incident photon
q	$=k-p_1-p_2$

[18] H. A. Bethe and W. Heitler, Proc. Roy. Soc. (London) A146, 83 (1934).

TABLE V. Theoretical estimates of asymmetric production.

E_0 (MeV)	$p_\pm$ (MeV/c)	θ (deg)	$B_1\times B_1$ Yield/V Eq. (9)	Quasi-elastic	Proton	Rad. corrns.	$B_1\times C^*$ [a] P_{33}	D_{13}	$B_1\times B_2$ [a]
390	170	30.0	7.28	0.049	0.048	0.056	−0.055	−0.013	0.008
	340	18.1	3.12	0.080	0.048	−0.010	0.055	−0.076	0.003
550	450	14.8	6.44	0.102	0.056	−0.002	0.110	−0.165	0.001
	450	20.4	0.91	0.316	0.100	−0.003	0.202	−0.298	−0.002
715	625	10.2	11.70	0.087	0.052	−0.014	0.075	−0.450	0.001
	625	13.0	2.83	0.196	0.078	−0.015	0.128	−0.760	−0.003
	625	15.0	1.16	0.340	0.101	−0.014	0.161	−0.966	−0.007

[a] Sign corresponds to electron detection.

form factors applicable to Eq. (4) are obtained:

$$f_{1p}(q^2)=\frac{2G^2}{1+r'}[1-r'(1+\kappa)^2],$$
$$f_{2p}(q^2)=\frac{G^2}{m^2(1+r')}[1+r'(1+\kappa)^2], \tag{7}$$

in which $r'=q^2/(4m^2)$, and terms of order r'^2 have been neglected.

Form factors for quasi-elastic production have been based on the expression obtained by Drell and Schwartz[19] and experimentally verified by Faissler and co-workers[20] in electron-carbon scattering. The quasi-elastic form factors reflect the relative probability that an electromagnetic interaction takes place with an individual nucleon of the target rather than coherently with the nucleus. The Drell-Schwartz sum rule for elastic and quasi-elastic electron interactions modifies the elastic form factor by the replacement

$$Z^2F^2\rightarrow G^2[Z+Z(Z-1)F^2+O(Z/m^2)],$$

in which $F^2(q^2)$ is the elastic nuclear form factor, $G^2(q^2)$ is the free proton form factor, and $O(Z/M^2)$ represents the largest of three correction terms for the conditions of this experiment. It amounts to about 1% of the preceding terms and has been neglected. Subtracting the carbon elastic term Z^2F^2 and substituting from Eqs. (6) and (7), the quasi-elastic form factors for the $B_1\times B_1$ cross section are

$$f_{1Q}(q^2)=f_{1p}[Z+(Z-1)f_1/2Z]-f_1,$$
$$f_{2Q}(q^2)=f_{2p}(m/M)^2[Z+(Z-1)M^2f_2/Z]-f_2. \tag{8}$$

The second of Eqs. (8) does not follow directly from (6) and (7). The additional factor of $(m/M)^2$ is required by the limiting form of the BDF form factors, $f_2(0)=Z^2M^{-2}$ and $f_{2p}(0)=m^{-2}$. If the proton and carbon contributions to the quasi-elastic yield are computed separately from Eq. (4), the appropriate mass term in the form factor cancels a similar term in the quantities $(p_i\cdot P)^2$ which appear in Eq. (4) and are closely approximated by $4E_i^2M^2$ or $4E_i^2m^2$. Addition of the factor $(m/M)^2$ simplifies computations by allowing the use of the carbon mass in Eqs. (3) and (4). Then $f_{1Q}(0)=f_{2Q}(0)=0$.

The estimate of $B_1\times B_1$ production in the plastic target is given by an integration of Eq. (3) over the unobserved lepton variables and the spectrometer acceptance. For events arising from carbon elastic, quasi-elastic, and from protons in the CH target the yield has been obtained by evaluation of the integral

$$Y(B_1\times B_1)=Q\int dp_1dp_2d\Omega_1d\Omega_2 \times d\sigma(B_1\times B_1: p_1,p_2,\theta_1\theta_2,\varphi_2) \tag{9}$$

using form factors from Eqs. (6), (7), and (8), respectively. The factor Q contains target and beam monitor parameters, and the spectrometer resolution was assumed to be sharp enough to allow the substitution $dp_2d\Omega_2\rightarrow\Delta p_2\Delta\Omega_2$ for the detected lepton. The effect of a finite photon beam has been suppressed in the integration since carrying out the integration using a realistic photon density distribution over the target produced an error of less than 0.01%.

The integrals were evaluated to a 1% convergence tolerance by Monte Carlo methods[21] and the results are listed in Table V. Column 4 gives the expected yield per volt of integrated primary beam current into a 1.003-μF capacitor for $B_1\times B_1$ production on carbon nuclei, and the remaining columns list other contributions as a fraction of the $B_1\times B_1$ yield on carbon. Yields from quasi-elastic and proton production are given in columns 5 and 6, respectively.

C. Contributions from $B_1\times B_2$ Interference

The interference between first and second Born Bethe-Heitler pair production amplitudes is expected to be a small correction to the $B_1\times B_1$ contribution. The relevant diagrams are shown in Figs. 1(a) and 1(d). Calculation of this term, while straightforward in principle, leads to a number of integrals for which exact

[19] S. D. Drell and C. L. Schwartz, Phys. Rev. 112, 568 (1958).
[20] W. L. Faissler, F. M. Pipkin, and K. C. Stanfield, Phys. Rev. Letters 19, 1202 (1967).
[21] J. M. Hammersley and D. D. Handscomb, *Monte Carlo Methods* (Wiley, New York, 1964).

solution is extremely difficult for spin-$\frac{1}{2}$ pair production. In the case of spin 0, however, calculations by Brodsky and Gillespie[22] have shown that the principal contribution from the three B_2 amplitudes derives from the first two graphs on the left of Fig. 1(d). Then by analogy with the arguments concerning the relative yield from the two B_1 graphs, the principal *electron* yield from $B_1\times B_2$ interference will be the result of interference between the middle graph of Fig. 1(d) and the right-hand graph of Fig. 1(a). In both graphs, the virtual electron coming off the incident photon vertex is almost on the mass shell, so that the ratio of yields, $B_1\times B_2/B_1\times B_1$, is given to a good approximation by the ratio of second Born interference to first Born elastic electron scattering cross sections. Similarly, the principal contribution to asymmetric *positron* production arises from interference between the left-hand graphs of Figs. 1(a) and 1(d), and the ratio of $B_1\times B_2/B_1\times B_1$ for this case is approximated by the ratio of second Born interference to first Born elastic positron scattering cross sections. Thus an estimate of the $B_1\times B_2$ pair production yield has been obtained by assuming

$$\sigma(B_1\times B_2)=(\pm R)\sigma(B_1\times B_1)\,, \tag{10}$$

where $\pm R$ is the ratio of second Born to first Born elastic scattering cross sections; positive for electron detection, negative for positron.

Calculations of the ratio R have been carried out by Lewis[23] assuming a static, spherically symmetric nucleus with a Yukawa charge distribution. Using Lewis's notation,

$$R=2Z\alpha\frac{K^2A_2}{a^2P^2}\left(\frac{k}{KA_1}(P^2+4k^2+2a^2)\arctan\frac{aK}{2A_1}\right.$$
$$\left.+\frac{2k}{K}\arctan\frac{2a^3}{K^3+3Ka^2}-\frac{P^2+4k^2+a^2}{A_2}\arctan\frac{a}{2K}\right), \tag{11}$$

with

$$A_1=(k^2K^2+4k^2a^2+a^4)^{1/2}$$

and

$$A_2=K^2+a^2.$$

In the context of elastic electron scattering, $\mathbf{K}$ is the three-momentum transfer to the nucleus, $\mathbf{P}$ is the sum of initial and final electron three-momenta, and k is the absolute value of the final electron three-momentum. For pair production, assuming detection of the electron, the momentum of the almost real virtual lepton coming from the real photon vertex assumes the role of the initial electron in the elastic scattering calculation. That is, $\mathbf{K}\to\mathbf{q}$, $\mathbf{P}\to\mathbf{q}+2\mathbf{p}_2$, and $K\to|\mathbf{p}_2|$. The terms in Eqs. (11) become

$$K^2\cong -q^2,$$
$$P^2\cong 4E_2^2-2(k\cdot p_2-k\cdot p_1-p_1\cdot p_2)\,, \tag{12}$$
$$k\cong E_2\,,$$

and those on the right are consistent with the definitions of Table IV. The Yukawa parameter has been assigned the value $a=173$ MeV/c by an empirical fit of the analytic form $F(q^2)=(1+q^2/a^2)^{-1}$ to the experimental carbon electromagnetic form factor.

The fractional contribution from this process has been calculated from the ratio of the integral

$$Y(B_1\times B_2)=Q\int dp_1dp_2d\Omega_1d\Omega_2$$
$$\times d\sigma(B_1\times B_1\colon p_1,p_2,\theta_1,\theta_2,\varphi_2)$$
$$\times R(p_1,p_2,\theta_1,\theta_2,\varphi_2) \tag{13}$$

to the value of the $B_1\times B_1$ yield of Eq. (9) using $d\sigma$ from Eq. (3), carbon form factors, and R from Eqs. (11) and (12). The ratios, listed in Table V, turn out to be relatively small compared with the experimental charge asymmetries and, above a nuclear momentum transfer of 0.3–0.4 F^{-2}, have a sign opposite to that observed.

D. Contributions from $B_1\times C^*$ Interference

As noted previously, the $B_1\times C$ interference terms are expected to be a factor of 10^{-3} lower than the $B_1\times B_1$ yield for photon energies below the first resonance. In the first resonance region, however, the interference may be enhanced by excitation of virtual π-N states in the Compton amplitude; specifically, the $\Delta(1236)$ and $N^*(1515)$ appear as logical possibilities from a phenomenological analysis of proton Compton scattering experiments.[24] Using the γNN^* coupling constant obtained by Dufner and Tsai,[25] Brodsky, Hearn, and Parsons[26] have calculated the $B_1\times C^*$ contribution assuming the formation of a virtual $\Delta(1236)$ in the Compton amplitude [Fig. 1(c)]. If the γNN^* vertex is dominated by the $M1$ transition, as experimentally supported, and if the final-state electron and positron are restricted to small angles ($\lesssim 20°$), their result for nuclear targets may be written

$$R^*=\frac{d\sigma(B_1\times C^*)}{d\sigma(B_1\times B_1)}\frac{8}{3}\frac{A}{Z}\frac{mC_3^2(0)}{M_3^3}\frac{X_1-X_2}{\lambda_{11}q^2(p_1+p_2)^2}$$
$$\times\frac{s-M_3^2}{(s-M_3^2)^2+\Gamma^2M_3^2}, \tag{14}$$

[22] S. J. Brodsky and J. R. Gillespie, Phys. Rev. **173**, 1011 (1968).
[23] R. R. Lewis, Jr., Phys. Rev. **102**, 537 (1956).
[24] S. Minami, Nuovo Cimento **47A**, 64 (1967).
[25] A. J. Dufner and Y. S. Tsai, Phys. Rev. **168**, 1801 (1968).
[26] S. J. Brodsky, A. C. Hearn, and R. Parsons, Phys. Rev. **187**, 1899 (1969).

where

$$X_1=\frac{1}{2k\cdot p_1}(E_1+E_2)(E_1^2+E_2^2)$$
$$\times[m^3+2mM_3^2+3M_3^3+2m^2(E_1+E_2)]$$
$$\times[q^2+\theta_1^2(E_1^2+E_1 2E_2)+\theta_2^2E_2^2],$$
$$X_2=X_1(p_1^\mu\leftrightarrow p_2^\mu),$$
$$s=(k+Q)^2,$$

M_3 and Γ are the resonance mass and width, and

$$q^2=-\mathbf{q}^2.$$

The only modification to the result of Ref. 26 has been the addition of the factor A/Z for the use of a nuclear target. The γNN^* coupling constant, $C_3^2(q^2)$, calculated in Ref. 25 using the N^* radiative decay width of Dalitz and Sutherland,[27] has been recalculated, yielding the result[28]

$$m^2C_3^2(0)=4.0\pm0.06,$$

which, strictly, is valid only at the $\Delta(1236)$ resonance peak. A kinematic correction factor for off-resonance c.m. energies is less than 10% of the stated value and has been neglected.

In the case of the $N^*(1515)$ resonance, more than one multipole amplitude has been found to contribute to the γNN^* transition, so that Eq. (14) would not necessarily yield valid results. A crude estimate of the second-resonance contribution to the interference term has been obtained, however, by substituting the N^* mass and width for those of the Δ and allowing the coupling constant to be a free parameter in fitting the experimental data.

Various forms of the resonance width were used to fit the data, including (a) the constant widths[29] of $\Gamma_0=120$ and 115 MeV for the $\Delta(1236)$ and $N^*(1515)$, respectively, and (b) energy-dependent widths of the form[25]

$$\Gamma=\Gamma_0(P_\pi^*/P_R^*)^{2L+1}, \quad (15)$$

where

$$P_\pi^{*2}=(km+\tfrac{1}{2}m_\pi^2)^2/s-m_\pi^2,$$
$$P_R^{*2}=(M_3^2-m^2+m_\pi^2)^2/4M_3^2-m_\pi^2,$$

and $L=1$, 2 for the first and second resonances, respectively. Additionally, the effect of resonance broadening due to nuclear absorption of the π-N state was considered in the manner of Ref. 26, by the replacement

$$\Gamma\rightarrow\Gamma+k/M_3\lambda, \quad (16)$$

in which k is the incident photon energy and λ is the mean free path of the resonance in nuclear matter. For the first and second resonances, the mean free paths in carbon computed from the total photoproduction cross sections are 2 and 8 F, leading to corrections of approximately 25 and 10%, respectively, to the unmodified widths.

The fractional contributions of the interference terms were calculated from the ratio of the integral

$$Y(B_1\times C^*)=Q\int dp_1dp_2d\Omega_1d\Omega_2$$
$$\times d\sigma(B_1\times B_1:p_1,p_2,\theta_1,\theta_2,\varphi_2)R^*(p_1,p_2,\theta_1,\theta_2,\varphi_2) \quad (17)$$

to the $B_1\times B_1$ result from Eq. (9). The calculated values of the fractional yields for the various experimental points are given in Table V which have been obtained by use of Eq. (15) for the resonance width, neglecting the effects of nuclear absorption broadening; this case turned out to provide the best fit to the experimental data. The sign of the interference contribution is clearly dominated by the term $(s-M_3^2)$, although at the 170 MeV/c, 30° experimental point, the negative value has been suppressed since the range of the integration over photon energies contains the zero of R^*. This is illustrated by Fig. 4, which shows the relative variation of the resonant factor of Eq. (14) with incident photon energy; the horizontal bars indicate the range of integration required for the four detected lepton momenta.

E. Radiative Corrections

The BDF calculations give radiative corrections to the $B_1\times B_1$ process in the form

$$\frac{\sigma_{\rm rad}}{\sigma(B_1\times B_1)}=\frac{\alpha}{\pi}\left[\ln\frac{2p_1\cdot p_2}{\mu^2}\left(\frac{13}{6}-\ln\frac{E_1E_2}{(\Delta E)^2}\right)\right], \quad (18)$$

in which $\Delta E=k_{\rm max}-k$, and $k_{\rm max}$ is the peak energy of the incident bremsstrahlung spectrum. The correction factors are given in Table V, column 7, as the ratio of the integral

$$Q\int dp_1dp_2d\Omega_1d\Omega_2\sigma(B_1\times B_1:p_1,p_2,\theta_1,\theta_2,\varphi_2)\frac{\sigma_{\rm rad}}{\sigma(B_1\times B_1)}$$

to the $B_1\times B_1$ yield given by Eq. (9).

F. Analysis and Comparison with Experimental Results

For each of the kinematic points listed by Table V, the estimated theoretical yield may be written in the

[27] R. H. Dalitz and D. G. Sutherland, Phys. Rev. **146**, 1180 (1966).

[28] In the notation of Ref. 25, the radiative decay width of the $\Delta(1236)$, taken from the analysis of electroproduction experiments of Ref. 27, should read $\Gamma_\gamma=\alpha Q^{*3}\mu^{*2}/(2M_pE_i^*)$ [Eq. (3.4)], with $\mu^*=(1.28\pm0.02)2\sqrt{2}\mu_p/3$. Then using the same assumption, namely, that the decay goes mainly by an $M1$ transition, Eq. (3.6) reads $\Gamma_\gamma=\alpha C_3^2(0)\frac{2}{3}Q^{*3}(E_i^*+M_p)/M_p$. Equating the two expressions, one obtains $C_3^2(0)=(8.48\pm0.13)(E_i^{*2}+E_i^*M_p)^{-1}$, which, using $E_i^*/M_p\approx1.04$ at the resonance center, yields the value given in the text.

[29] N. Barash-Schmidt, A. Barbaro-Galtieri, L. R. Price, A. H. Rosenfeld, P. Söding, C. G. Wohl, M. Roos, and G. Conforto, Rev. Mod. Phys. **41**, 109 (1969).

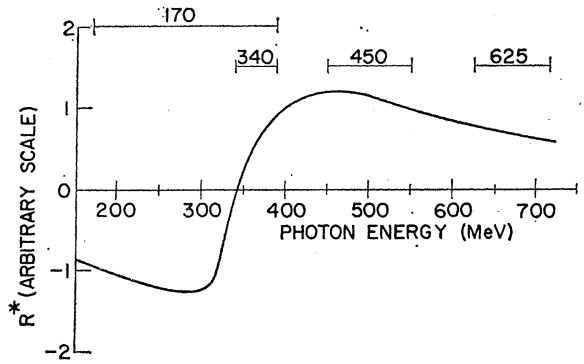

FIG. 4. Relative variation of the Compton interference term R^* in the region of the $\Delta(1236)$ resonance. The horizontal bars indicate the range of photon energies contributing to the observed yield, and the numbers attached give the momentum of the detected lepton in MeV/c.

form

$$Y(e^{\pm})=Y(B_1\times B_1)\times[1+R_{\text{even}}\mp(R_{12}+a_1R_{33}+a_2R_{13})], \quad (19)$$

in which $Y(e^{\pm})$ is the theoretical positron (electron) yield, R_{even} represents a sum of the ratios of quasi-elastic, proton, and radiative correction terms, even under charge conjugation, and R_{12} is the $B_1\times B_2$ interference ratio, odd under charge conjugation. R_{33} and R_{13} are the odd contributions from the Compton amplitude, Eq. (14), and the a_i are constants determined from a best fit to the experimental data. The expected charge asymmetry, using Eq. (19), is

$$A=\frac{Y(e^-)-Y(e^+)}{Y(e^-)+Y(e^+)}=\frac{R_{12}+a_1R_{33}+a_2R_{13}}{1+R_{\text{even}}}. \quad (20)$$

Table VI lists a comparison of the a_i derived from assuming (a) a constant width, (b) an energy-dependent width, and (c) an energy-dependent width plus a correction for resonance broadening. Because of the scatter in the experimental asymmetries, the errors on the a_i and the associated χ^2 values are relatively large, but the data indicate a slight preference for (b). The data agree with the predictions of Eq. (14) in the case of the first-resonance contribution; however, regardless of width assumption, the asymmetry contributed by the second resonance is consistent with zero. Thus, the calculation of theoretical yields given in Table VII assumes the values $a_1=1$ and $a_2=0$ and uses the energy-dependent width relation, Eq. (15), without nuclear absorption broadening corrections.

TABLE VI. Effect of resonance width assumptions.

	Constant width (Ref. 29)	Energy-dependent widths Eq. (15)	Energy-dependent widths Eqs. (15) and (16)
a_1	0.28±0.26	1.05±0.47	1.13±0.59
a_2	−0.14±0.24	−0.03±0.12	−0.45±0.15
χ^2	17.9	15.4	16.3

V. DISCUSSION AND CONCLUSIONS

The ratios of experimental to theoretical results shown in Table VII indicate general agreement of the experiment and theory. The values of R(expt/theor) essentially represent the consistency of the data with the predictions of QED for the case of asymmetric detection geometry, and, assuming that the contributions from the "bad" diagram of Fig. 1(a) agree with the point-interaction hypothesis of QED, the ratio of experiment to theory may be written as

$$\text{expt/theor}=(0.95\pm0.06)-\tfrac{1}{5}(0.3\pm0.82)|q^2|,$$

from which a 68% level of confidence limit on the cut-off parameter gives $\Lambda<1.06$ F. In addition to the statistical errors given in this expression, the systematic errors have been estimated to be less than 7.3%. Without consideration of the validity of QED, the ratio may be written as

$$\text{expt/theor}=(0.95\pm0.06)-(0.06\pm0.16)|q^2|,$$

indicating no significant q^2-dependent systematic errors, a verification of the BDF formulation of asymmetric pair production and the Drell-Schwartz quasi-elastic sum-rule contributions which become an appreciable fraction of total production at the larger nuclear momentum transfers.

The results shown in Table VII also indicate that observed charge asymmetries can be explained principally by the $B_1\times C^*$ interference term with the assumption of a virtual $\Delta(1236)$ state in the Compton amplitude. The primary feature of this term would be a sharp reversal of the sign of the charge asymmetry at the zero of the P_{33} amplitude, corresponding to an incident photon energy of 340 MeV. Unfortunately, the only experimental point obtained in this region represented an average of photon energies over the interval 170–390 MeV, resulting in a small and statistically unreliable positron excess as expected from the theoretical cross section. For the remaining experimental points, the cross section predicts the observed electron excess, and the conclusions about the validity of Eq. (14) are weighted heavily by these results, not only because of their number but because of their relatively small statistical errors. On this basis, the data show a slight preference (Table VI) for the energy-dependent resonance width, Eq. (15), but conclusions concerning the validity of the width corrections for absorption of the resonance in nuclear matter remain subject to further investigation. The results of the present experiment cannot rule out their applicability.

Using the values of a_1 and a_2 from Table VI, the best fit to the data yields a value of the γNN^* coupling constant of $mC_3(0)=2.1\pm0.9$ for the first resonance. The error on this result is too large to allow a distinction

TABLE VII. Comparison of experimental and theoretical results.

E_0 (MeV)	$p_\pm$ (MeV/c)	θ (deg)	Polarity	Expt yield/V	Theor yield/V	$R_{(\text{expt/theor})}$	A_{theor} Eq. (20)	A_{expt}	$A_{(\text{expt/theor})}$
390	170	30.00	+	8.74±0.95	8.55	1.02±0.11	−0.041	−0.05 ±0.08	1.2 ±1.9
			−	7.90±0.96	8.24	0.96±0.12			
	340	18.10	+	3.24±0.22	3.36	0.96±0.07	0.052	0.21 ±0.05	4.0 ±1.0
			−	4.92±0.37	3.61	1.36±0.10			
550	450	14.85	+	6.36±0.44	6.84	0.93±0.06	0.096	0.063±0.053	0.66±0.55
			−	7.21±0.57	8.04	0.90±0.07			
		20.40	+	1.13±0.12	1.16	0.97±0.10	0.142	0.092±0.072	0.65±0.51
			−	1.36±0.13	1.41	0.96±0.09			
715	625	10.15	+	7.82±0.92	12.31	0.64±0.08	0.068	0.270±0.112	4.0 ±1.6
			−	13.59±2.2	14.02	0.97±0.16			
		13.00	+	2.91±0.28	3.28	0.89±0.09	0.099	0.041±0.068	0.41±0.69
			−	3.16±0.30	3.84	0.82±0.08			
		14.95	+	1.36±0.16	1.52	0.90±0.11	0.108	0.176±0.076	1.6 ±0.7
			−	1.94±0.19	1.80	1.08±0.11			

between the $SU(6)$ prediction of 1.61 or the prediction of the value 2.2 from the Chew-Low static theory.[30]

For the case of the second resonance, the data are consistent with the conclusion that the Compton amplitude with excitation of an $N^*(1515)$ virtual state is purely imaginary. The best estimate of the coupling constant for this vertex is $mC_3(0) = -0.06 \pm 0.24$.

In conclusion, it has been shown that (1) asymmetric electron pair production in the region of the first two pion-nucleon resonances in general agreement with known QED processes, (2) charge-asymmetric production cross sections agree with predictions of the interference calculations using the isobar model and yield asymmetries about 10^2 greater than those expected from the low-energy Thomson limit, and (3) interference between first and second Born approximation pair production is a relatively small contribution to the total charge asymmetry in this region.

[30] Reference 25 contains discussion and references to these alternative predictions.

ACKNOWLEDGMENTS

The authors wish to express their gratitude to Professor D. M. Ritson and Dr. B. Gittelman for many useful discussions on experimental topics; to Professor A. C. Hearn and Dr. S. J. Brodsky, Dr. J. R. Gillespie, and Dr. R. Parsons for their invaluable contributions toward the theoretical interpretation of the results; and to the staff of W. W. Hansen Laboratories of Physics for their assistance in construction of the experimental apparatus and for efficient operation of the accelerator.